

REGULAR BREAKING WAVES PAST A SUBMERGED BERM

Luca Chiapponi ¹, Maria Clavero ², Miguel A. Losada & ²Sandro Longo ¹

(1) Dipartimento di Ingegneria Civile, dell'Ambiente, del Territorio e Architettura (DICATeA), Università di Parma, Parco Area delle Scienze, 181/A, 43124 Parma, Italy; (2) Instituto Interuniversitario de Investigación del Sistema Tierra, Universidad de Granada, Avda. del Mediterráneo s/n, 18006 Granada, Spain

KEY POINTS:

- The velocity fields induced by regular breaking waves past a fixed bar on a 1:10 rigid plane slope were measured and analysed using a volumetric particle-tracking velocimetry system.
- The linear momentum is generally positive during breaking (transfer toward the crest) and negative immediately after breaking (transfer from the crest toward the underlying flow field).
- The average pressure gradient during breaking influences the profile of the breaker.

1 INTRODUCTION

Waves and breaking waves are a dominant component of the surface of seas and lakes and play an important role in gas, heat and chemical exchanges at the interface between water and air. Breaking is almost always present in shallow water where it is induced by bathymetry. Breaking occurs in random locations, even if the waves are periodic and regular, such as in a laboratory flume. If a submerged bar is present, either natural or man-made, the breaking section for regular waves is nearly deterministic because the bar forces the instability. However, even though bars force the regular appearance of breakers, the phenomenon preserves an intrinsic non-deterministic variability in its flow structure and in the overall geometry.

The aims of the present work are the analysis of the flow field in the breaker, the quantification of the terms in the equations usually adopted for modelling the flow and the turbulence, the identification of the level of isotropy/anisotropy in the turbulence (not detailed in the present paper), and the analysis and balance of vorticity and the coherent structures (not detailed in the present paper). The data presented here refer to a diffuse natural cross-shore geometry, where a sand bar naturally develops on an inclined submerged beach profile as a consequence of sediment transport induced by currents and breaking waves.

2 EXPERIMENTAL APPARATUS AND EXPERIMENTS

The experiments were conducted in the wave flume located in the Laboratorio de Dinámica de Fluidos Ambientales of the CEAMA (Centro Andaluz de Medio Ambiente) in Granada. The flume is 23 m long, 100 cm high, and 65 cm wide. A sketch of the flume is shown in Figure 1(a).

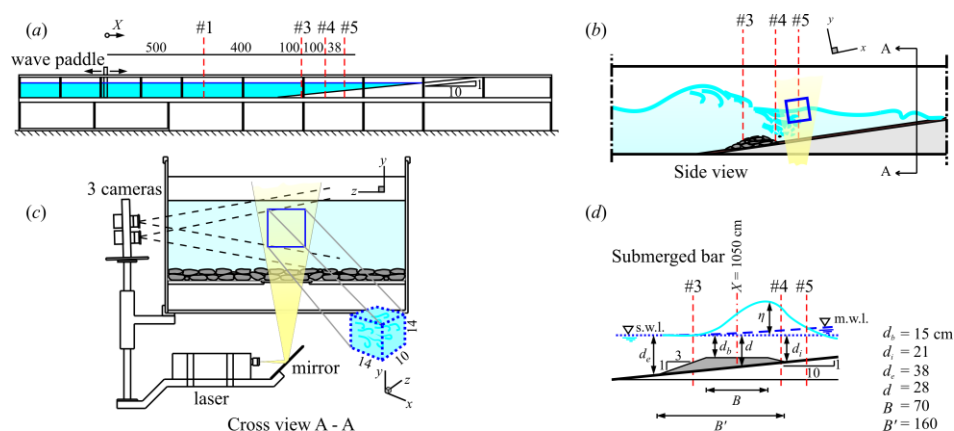


Figure 1. The experimental flume: (a) side view of the flume; (b) layout of the bar and of the volume of measurement; (c) cross view of the flume; (d) the geometry of the bar, characterized by $d_b/d = 0.54$, where $d = 28$ cm is the still water depth in the mid-section of the bar ($X = 1050$ cm). The dot line indicates the still water level, the dashed line is the mean water level (wave set-up or set-down). Dimensions are in centimetres.

At one end of the flume, a piston-type wave maker is equipped with an active wave absorption control system (AWACS) for the absorption of the reflected waves. An artificial slope of 1:10 was built starting at $X = 900$ cm (the origin of the external coordinate system X is the mid-position of the wave paddle), with a berm of stones and plastic blocks usually used in physical models of berm breakwaters at $X = 1050$ cm, with a crest ≈ 70 cm wide and ≈ 15 cm beneath the still water level, see Figure 1(d). A glass window was positioned at the bottom in the measuring section to allow laser penetration. The camera system (V3V by TSI Inc.) was positioned with a side view of the flume and the volume of measurements was a cube with a side length equal to ≈ 14 cm in the cross-shore and vertical directions and to ≈ 10 cm in the alongshore direction, and it was centred at $X = 1138$ cm in the middle of the channel. In this paper, all the experimental data are presented in the local coordinate system $x - y - z$. The surface elevation during tests was measured in several sections (see Figure 1(a)), including the section of the breaker, using Ultrasonic probes (UltraLab® USL 80D by General Acoustics, sensor model USS635, accuracy on the instantaneous water level measurements equal to ≈ 0.5 mm) with data acquired at 200 Hz. The acquisition of the V3V images was controlled by the signal of probe in Section 4, where the internal toe of the bar was positioned. Nine different experiments were performed with regular first-order Stokes waves with the periods $T = 1.5, 2.0$ s and target wave height (almost coincident with the generated wave height) $H_0 = 6, 7, 8, 9$ and 10 cm. According to the values of the Iribarren number, defined as $\xi_0 = \tan\alpha / \sqrt{H_0/L_0}$ with α the bed slope, the breakers should be plunging ($0.5 < \xi_0 < 3.3$); however, the presence of the bar induced breaking, resulting in the spilling type.

For each wave test, 10 sequences were acquired, with each sequence containing 10 or 13 shots (for the 1.5 s and the 2.0 s period waves, respectively) acquired at the maximum allowed frequency, i.e., 7.25 Hz.

Experimental data in planar PIV and in V3V require the elimination of background noise, the detection of outliers and the filling of gaps due to missing data. Among the various techniques (see *Kitzhofer et al. 2011*), we chose the “snapshot” Proper Orthogonal Decomposition (POD) as introduced by *Sirovich (1987)*. The signal is analysed to detect the best base described by several modes, and each snapshot can be reconstructed as a linear combination of the elements of the base (the modes). The number of modes in the POD technique is equal to the number of snapshots available. The modes can be ranked according to their energy contribution, and the reconstruction includes a limited number of modes, in most cases those containing at least 90% of the total energy, without residual modes containing more than 1% of the total energy.

Figure 2 shows the instantaneous velocity vectors, the phase-averaged velocity and the fluctuating component (the difference between the instantaneous and the phase-averaged velocity) for a snapshot of Experiment 6b ($H_0 = 6$ cm, $T = 2$ s). For clarity, only the data in the $x - y$ vertical plane in the mid-section of the flume ($z = 0$) are presented.

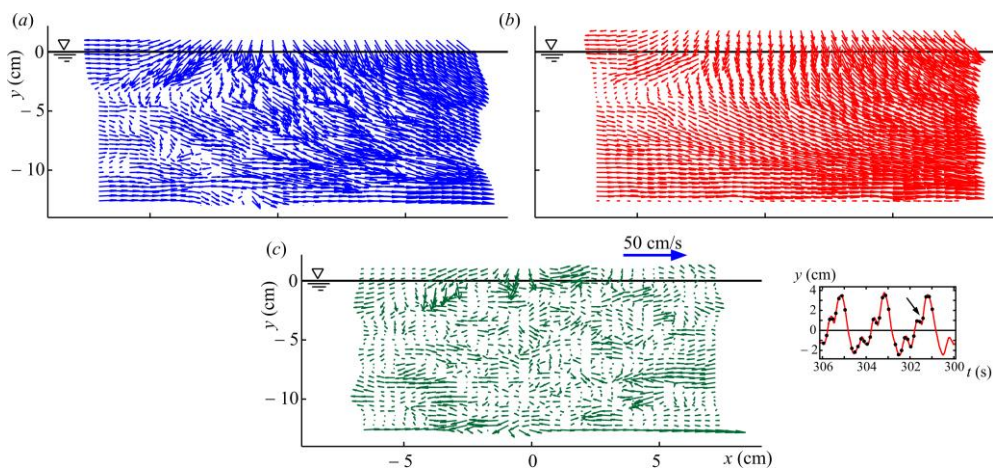


Figure 2. Experiment 6b, the fourth shot in a sequence of 13 shots of the first measured wave cycle. (a) Instantaneous velocity in the mid plane of the flume ($z = 0$); (b) phase-averaged velocity, and (c) velocity vectors difference (fluctuating velocity) between the instantaneous velocity and the phase-averaged velocity. Only velocity components in the $x - y$ plane are shown. The inset depicts the surface elevation time series with the symbols indicating the time of the shot.

3 RESULTS AND DISCUSSION

Adopting the Reynolds decomposition, the main variables in a turbulent flow, velocity components and pressure, are separated into an (phase-)average value and the fluctuation:

$$u_i = \tilde{u}_i + u'_i, \quad p = \tilde{p} + p' \quad (1)$$

where $i = 1, 2, 3$, ($x - y - z$). The phase-averaged velocity \tilde{u}_i is the organised part of the flow and in the present analysis includes the time-averaged velocity (the undertow below the trough level). The equations of motion for the average flow in an incompressible fluid are

$$\underbrace{\frac{\partial \tilde{u}_i}{\partial t}}_{I_m} + \underbrace{\tilde{u}_j \frac{\partial \tilde{u}_i}{\partial x_j}}_{II_m} = - \underbrace{\frac{1}{\rho} \frac{\partial \tilde{p}}{\partial x_i}}_{III_m} + \underbrace{g_i}_{IV_m} + \underbrace{\frac{1}{\rho} \frac{\partial \tilde{\tau}_{ij}}{\partial x_j}}_{V_m} - \underbrace{\frac{\partial \widetilde{u'_i u'_j}}{\partial x_j}}_{VI_m} \quad (2)$$

where ρ is the mass density of the fluid, g_i is the i th component of the acceleration of gravity, τ_{ij} is the stress tensor due to the viscosity. The term $u'_i u'_j$ represents the Reynolds stress tensor. The terms in eq.(2) are conventionally defined as local inertia (I_m), advection (II_m), gradient pressure (III_m), gravity contribution (IV_m), viscous stresses contribution (V_m), and turbulent stresses contribution (VI_m). The gravity term is negated by considering the pressure field which excludes the hydrostatic effect; hence, the sum of the gradient pressure and the gravity contribution ($III_m + IV_m$) is the net gradient pressure. We take advantage of the availability of measurements of three velocity components in several points in space and at different times to estimate all the terms in eq.(2). The results are presented in non-dimensional form with a vertical length scale given by the mean water depth $d + \bar{\eta}$, where d is the still-water depth and $\bar{\eta}$ is the time-averaged surface elevation. The velocity scale is given by $\sqrt{g(d + \bar{\eta})}$, and the time scale is given by the wave period T . The horizontal length scale is $T\sqrt{g(d + \bar{\eta})}$. Surface elevations are measured from the mean water level; hence, $\zeta = (y - \bar{\eta})/(d + \bar{\eta})$.

Four of the six terms in the linear momentum balance equation in the cross-shore direction were directly estimated. Local inertia is generally dominant, with advection on a smaller order of magnitude, except immediately after breaking. Additionally, the turbulent (Reynolds) stress contribution becomes relevant essentially during breaking, whereas the viscous stress contribution is three orders of magnitude smaller than all other contributions. The net gradient pressure term (excluding the hydrostatic component), was computed by summing all the estimated terms. The phase resolved contributions integrated in the vertical are shown in Figure 3 for the cross-shore (x), the vertical (y) and the alongshore (z) directions.

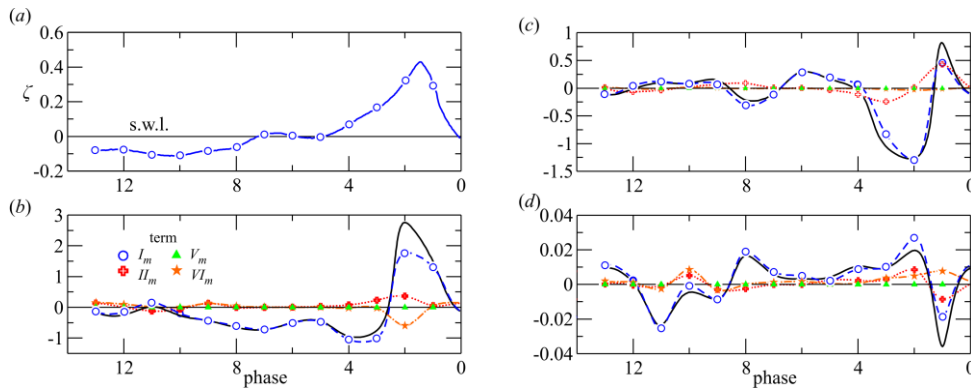


Figure 2. Experiment 9b ($H_0 = 9$ cm, $T = 2$ s). (a) Phase-averaged surface elevation; (b) terms in linear momentum balance in the cross-shore direction, (c) in the vertical direction, and (d) in the alongshore direction. The dashed line refers to local inertia (I_m), the dotted line refers to advection (II_m), the dash-dotted line refers to turbulent stress contribution (VI_m), and the solid line indicates the net gradient pressure. The triangles represent the viscous term contribution (V_m) which is almost negligible in all the three directions.

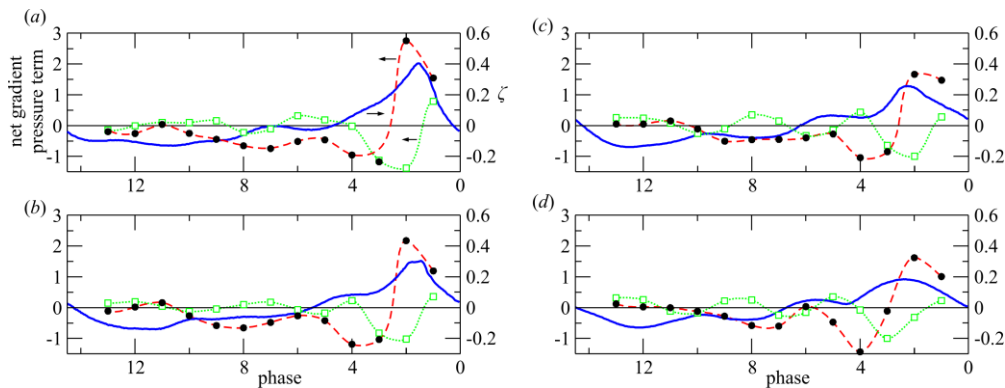


Figure 4. Net gradient pressure term in the x (cross-shore) and y (vertical) directions, and breaking wave profile for Experiments 9b-8b-7b-6b (panels a-b-c-d). The solid blue line is the wave profile (referred to the right vertical axis), filled circles (dashed red line) are the estimated net pressure gradient term in the cross-shore direction, empty squares (dot green line) are the estimated net pressure gradient term in the vertical direction. The net pressure gradient terms are referred to the left vertical axis.

In the cross-shore direction (Figure 3b), for most of the wave cycle the net gradient pressure balances only local inertia because advection and the turbulent stress contribution are negligible. Only beneath the crest does the gradient pressure act against local inertia, advection and turbulent stresses, and it is equal to approximately three times the gravity component parallel to the bottom or one-fourth the value of gravity. For plunging breakers, the peak gradient pressure is much stronger, up to $5g$ (see, e.g., *Peregrine 1983*). We recall here that the present data are missing the peak values. In the vertical direction (Figure 3c), advection is comparable to local inertia immediately before breaking, with positive values, and the subsequent phases are almost completely dominated by local inertia. Turbulent stresses play a minor role with respect to the cross-shore dynamics, and viscous stresses are negligible. In the alongshore direction (Figure 3d), all terms are much smaller than in the other two directions. In the presence of a rigorous symmetry, flat profiles were expected for all the terms, and the presence of a periodic variation in the inertial terms clearly indicates that alongshore dynamics are triggered by instabilities of various origins, including systematic asymmetries in the breaker, which is a three-dimensional phenomenon. It is expected that in larger flumes these three-dimensional effects are more evident. Notably, the inertial terms and turbulent stresses are comparable during the entire wave cycle. The gradient pressure term is considered a key element in the shape of the profile of the breaker. It achieves the highest values during steepening of the wave crest and strongly contributes to the aspect of the breakers and to the post-breaking wave profile evolution.

Figure 4 (a,b,c,d) shows the net pressure gradient terms in the x and y directions for the $T = 2.0$ s wave tests. The net pressure gradient term in both directions oscillates following the wave profile but with a phase shift, being zero several times and being the cross-shore one the largest in most cases (but not as large as it should be expected). A steep front (Figure 4a,b) is forced by the large positive value of the cross-shore pressure gradient with a peak value delayed with respect to the wave crest; the delay is reduced for smaller wave breaking height (Figure 4c,d). Steepening of the wave front is strongly correlated to the cross-shore net pressure gradient term, while smoothening of the wave profile is correlated with the vertical component of the net pressure gradient. The results for the other waves (with period $T = 1.5$ s) are similar (not shown).

REFERENCES

- Kitzhofer, J., Nonn, T. & Brcker, C. 2011 Generation and visualization of volumetric PIV data fields. *Experiments in Fluids* 51 (6).
- Longo, S. 2012 Wind-generated water waves in a wind tunnel: Free surface statistics, wind friction and mean air flow properties. *Coastal Engineering* 61 (1), 27-41.
- Longo, S., Petti, M. & Losada, I.J. 2002 Turbulence in the swash and surf zones: a review. *Coastal Engineering* 45 (34), 129-147.
- Nadaoka, K., Hino, M. & Koyano, Y. 1989 Structure of the turbulent flow field under breaking waves in the surf zone. *Journal of Fluid Mechanics* 204, 359-387.
- Peregrine, D.H. 1983 Breaking waves on beaches. *Ann. Rev. Fluid Mech.* 15, 149-178.
- Petti, M. & Longo, S. 2001 Turbulence experiments in the swash zone. *Coastal Engineering* 43 (1), 1-24.
- Sirovich, L. 1987 Turbulence and the dynamics of coherent structures. Part I, II and III. *Quart. Appl. Math.* XLV(3), 561-590.
- Tennekes, H. & Lumley, J.L. 1972 *A first course in Turbulence*. Cambridge University Press.